Pharm Res (2015) 32:1002–1016
DOI 10.1007/s11095-014-1512-2

RESEARCH PAPER

Liposome Encapsulated Albumin-Paclitaxel Nanoparticle for Enhanced Antitumor Efficacy

Hima Bindu Ruttala • Young Tag Ko

Received: 5 June 2014 / Accepted: 3 September 2014 / Published online: 12 September 2014

ABSTRACT

Purpose Albumin nanoparticles have been explored as a promising delivery system for various therapeutic agents. One limitation of such formulations is their poor colloidal stability *in vivo*. Present study aimed at enhancing the chemotherapeutic potential of paclitaxel by improving the colloidal stability and pharmacokinetic properties of albumin-paclitaxel nanoparticles (APNs) such as Abraxane®.

Methods This was accomplished by encapsulating the preformed APNs into PEGylated liposomal bilayer by thin-film hydration/extrusion technique.

Results The resulting liposome-encapsulated albumin-paclitaxel hybrid nanoparticles (L-APNs) were nanosized (~200 nm) with uniform spherical dimensions. The successful incorporation of albumin-paclitaxel nanoparticle (NP) in liposome was confirmed by size exclusion chromatography analysis. Such hybrid NP showed an excellent colloidal stability even at 100-fold dilutions, overcoming the critical drawback associated with simple albumin-paclitaxel NP system. L-APNs further showed higher cytotoxic activity towards B16F10 and MCF-7 cells than APN; this effect was characterized by arrest at the G_2/M phase and a higher prevalence of apoptotic subG_1 cells. Finally, pharmacokinetic and biodistribution studies in tumor mice demonstrated that L-APNs showed a significantly enhanced plasma half-life, and preferential accumulation in the tumor.

Conclusions Taken together, the data indicate that L-APNs can be promising therapeutic vehicles for enhanced delivery of PTX to tumor sites.

KEY WORDS albumin nanoparticle · colloidal stability · liposome · paclitaxel · pharmacokinetic

ABBREVIATIONS

APNs	Albumin-paclitaxel nanoparticles
CLSM	Confocal laser scanning microscopy
DLS	Dynamic light scattering
DSC	Differential scanning calorimetry
FACS	Fluorescence Activated Cell Sorting (Flow Cytometry)
HPLC	High performance liquid chromatography
L-APNs	Liposome-encapsulated albumin-paclitaxel hybrid nanoparticles
LC-MS/MS	Liquid chromatography-tandem mass spectrometry
NP	Nanoparticle
PTX	Paclitaxel
XRD	X-ray diffraction

INTRODUCTION

Paclitaxel (PTX), a classical microtubule inhibitor, works by promoting tubulin polymerization and microtubule stabilization, resulting in the arrest of mitosis at the G_2-M phase and mitotic cell death (1,2). However, the poor aqueous solubility of PTX (less than 1 μg/ml) limits its use in the natural form (3,4), requiring that PTX is formulated in a mixture of Cremophor EL/absolute ethanol (1:1 v/v, Taxol®) to solubilize the drug for intravenous (i.v.) injection (2,5). This vehicle is associated with serious side effects attributable mainly to Cremophor EL (6). As a result, various formulation strategies have been evaluated to alleviate vehicle-related side effects and at the same time improve the chemotherapeutic efficacy of PTX. Notably, much interest has been focused on developing nanotechnology-based PTX formulation strategies such

Electronic supplementary material The online version of this article (doi:10.1007/s11095-014-1512-2) contains supplementary material, which is available to authorized users.

H. B. Ruttala • Y. T. Ko (✉)
College of Pharmacy, Gachon University, 191 Hambakmoero Yeonsu-gu, Incheon 406-799, Republic of Korea
e-mail: youngtakko@gachon.ac.kr

as emulsions (7), polymeric micelles (8), solid lipid nanoparticles (9), liposomes (10), nanoparticles (11), PTX-polymer conjugates (12).

In 2006, the FDA approved Abraxane®, a Cremophor®-free formulation of human serum albumin-bound PTX nanoparticles (average size of 130 nm) for treating recurrent metastatic breast cancer (13,14). Although, Abraxane® has been shown to improve the tumor response, the pharmacokinetic properties of Abraxane® are no better than those of the Taxol® formulation (14). This may be due to the poor colloidal stability of Abraxane® during blood circulation. Indeed, upon i.v. injection and subsequent dilution in the large volume of blood, Abraxane® disassembles, allowing PTX to dissociate and resulting in a concentration curve and nonspecific biodistribution similar to those associated with free PTX (5,15). Consequently, there is a tremendous interest in developing intelligent delivery systems that can maintain their nanostructure assembly during circulation, thus providing sustained blood levels. Such systems would be preferentially distributed into tumor tissues by so called enhanced permeability and retention (EPR) effect and thus maximize the therapeutic efficacy of PTX while minimizing side effects.

Liposomes represent a versatile and advanced nanodelivery system for a wide range of active therapeutics (16,17). Liposomes, in particular PEGylated liposomes, have been successfully applied to endow a prolonged blood circulation to the therapeutic agents with poor pharmacokinetic behavior such as doxorubicin (Doxil®), amphotericin (Ambiosome®), daunorubicin (Daunoxome®) due to their characteristic *in vivo* stability. Liposomal encapsulation can be applied to various macromolecular therapeutics such as peptides (18) nucleic acids (19) and nanoparticles (20) as well. Recently we reported the liposome-encapsulated polyethylenimine/ oligonucleotide polyplexes to improve the poor *in vivo* behavior of polyplexes (21).

Therefore, it could be proposed that encapsulation of the albumin-PTX nanoparticles (APNs) within a lipid liposome bilayer could, in principle, markedly improve the plasma pharmacokinetic and biodistribution profile of albumin and PTX, resulting in augmented pharmacological features. This type of liposome-encapsulated albumin-PTX nanoparticles (L-APNs) would be expected to permeate tumor capillaries and extravasate into the fenestration of tumor tissues *via* the enhanced permeability and retention (EPR) effect (22). In the present study, we attempted to apply the same approach of liposomal encapsulation to provide the otherwise unstable APNs with *in vivo* stability (Fig. 1). We hypothesized that the liposomal encapsulation of the APNs would improve colloidal stability and prolong blood circulation, thereby alleviating the poor qualities of free PTX or APN. To accomplish this, we prepared the APNs by a desolvation technique, followed by encapsulation into liposome bilayers *via* thin-film hydration. The resulting L-APNs were evaluated with respect to physical characterization, *in vitro* dissolution and stability and *in vivo* pharmacokinetics.

MATERIALS AND METHODS

Materials

PTX was purchased from TCI Co., LTD (Tokyo, Japan). Bovine serum albumin (MW=66,000) and 3-(4, 5-dimethylthiazol-2-yl)-2,5-diphenyl tetrazolium bromide (MTT) were procured from Sigma-Aldrich (Yongin, South Korea). 1-Palmitoy-2-oleoyl-*sn*-glycero-3-phosphocholine (POPC), dioleoyl-1,2-diacyl-3-trimethyl ammonium propane (DOTAP), 1,2-distearoyl-*sn*-glycero-3-phosphoethanolamine-*N*--[methoxy(polyethylene-glycol)-2000] (DSPE-PEG2000), and cholesterol were purchased from Avanti Polar Lipids (Alabaster, AL, USA). All other chemicals were of reagent grade and were used as supplied.

Preparation of Albumin-Paclitaxel Nanoparticles (APNs)

APNs were prepared using a desolvation technique. Briefly, albumin was dissolved at a concentration of 1 mg/ml in distilled water, filtered through a 0.45 μm filter (PVDF syringe filter, 13 mm, CHROMDISC^{TM}, Korea), and adjusted to pH 9 by using 0.2 M NaOH. PTX was separately dissolved at a concentration of 13 mg/ml in 100% ethanol. Ten microliters of the PTX solution was mixed with 200 μl of the albumin solution by dropwise addition over 30 min with stirring, followed by sonication for 1.5 h. The final formulation included 1% ethanol (23,24).

Preparation of Liposome-Encapsulated APNs (L-APNs)

The POPC (6 μmol), cholesterol (3.0 μmol), DOTAP (1 μmol), and DSPE-PEG2000 (0.3 μmol) lipids were dissolved in chloroform, followed by removal of chloroform using a rotary evaporator. The APN solution (1 mL) was then added to the dried cationic lipid film and the mixture was incubated at room temperature for 4 h with intermittent mixing, resulting in a final lipid concentration of 10 mM. The suspension was extruded 11 times through a stack of two polycarbonate membranes of 200 nm in pore size by using an Avanti Mini Extruder (Avanti Polar Lipids, USA).

Measurement of Hydrodynamic Size, ζ-Potential, and Morphology

The hydrodynamic size, polydispersity index (PDI), and ζ-potential was analyzed using dynamic light scattering (DLS). The nanoparticle and liposomal dispersions were suitably

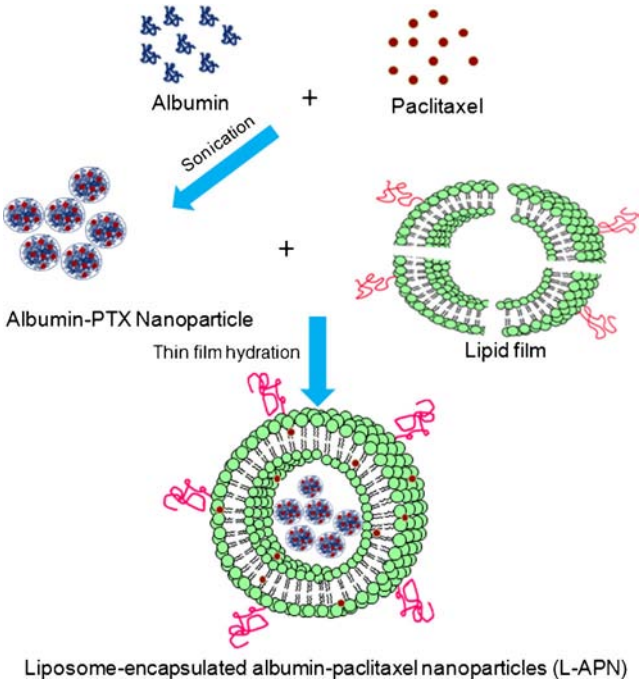

Fig. 1 Schematic representation of liposome-encapsulated albumin-paclitaxel nanoparticles (L-APN).

diluted with distilled water and measured at 25°C in ELS-Z (Photal, Osaka, Japan). The morphologies of the different formulations were examined using a transmission electron microscope (TEM; H7600, Hitachi, Tokyo, Japan) at an accelerating voltage of 100 kV.

Characterization of the Physical State of Nanoparticle Formulations

A differential scanning calorimeter (DSC-Q200, TA Instruments, and New Castle, DE, USA) was used to study the thermal behavior of the samples. Differential scanning calorimetry (DSC) scans were recorded at a heating rate of 10°C/min, ranging from 40°C to 250°C. X-ray diffraction (XRD) patterns for the samples were recorded using a vertical goniometer and an X-Ray diffractometer (X'Pert PRO MPD diffractometer, Almelo, The Netherlands).

FT-IR spectra were recorded using a Thermo Scientific Nicolet Nexus 670 FT-IR Spectrometer and Smart iTR software with a diamond window (Thermo Fisher Scientific Inc., Waltham, MA). Spectra were recorded from 550 to 4,000 cm^{-1} at a resolution of 4 cm^{-1}, 32 scans per sample.

Measurement of Drug Loading and Encapsulation Efficiency

Drug loading efficiency was determined by performing HPLC after ultra-filtration using an Amicon centrifugal filter device (molecular weight cut off [MWCO], 10,000 Da, Millipore, Billerica, MA, USA). Twenty micro liters of the filtered sample was injected into a C18 column (Sepax BR-C18, 5 μm 120 Å 4.6×150 mm). The mobile phase was a 1:1 mixture of acetonitrile and water with a flow rate of 1.0 mL/min. To evaluate the non-encapsulated PTX, we filtered 500 μL of the liposomal formulation *via* centrifugal ultrafiltration for 30 min at 14,000 rpm. The amount of PTX in the filtrate was determined using HPLC with UV monitoring at 227 nm. Drug loading and encapsulation efficiency were calculated using the following formulas:

$$\text{Encapsulation Efficiency(EE)} = \frac{\text{Total amount of PTX} - \text{Amount of free PTX}}{\text{Total amount of PTX}} \times 100$$

$$\text{Loading Efficiency(LE)} = \frac{\text{Total amount of PTX} - \text{Amount of free PTX}}{\text{Total weight of Lipids}} \times 100$$

Measuring Drug Release *In Vitro*

PTX release from the formulations was measured by dialysis method. The concentration of PTX in each sample was measured by performing liquid chromatography-tandem mass spectrometry (LC-MS/MS) using an Agilent HPLC (1260 series, USA) connected to a 6490 Triple quadrupole mass spectrometer equipped with an ESI Agilent jet stream ion source. Detail methodology in Supplementary (SM 1).

Colloidal Stability Studies

The colloidal stability of the formulations was assessed by DLS for 1 month upon storage in the refrigerator (4°C) or at ambient room temperature (25°C). Dilution-induced dissociation was assessed using a size-exclusion column (Zenic SEC-300, 3 μm 300 Å, 4.6×150 mm) at different dilutions. Supplement (SM 2).

Cellular Uptake Studies

The cellular uptake of the formulations was evaluated in mouse melanoma cells (B16F10) and human breast cancer cells (MCF-7) by qualitative and quantitative methods using confocal laser scanning microscopy (CLSM), flow cytometry, and LC-MS/MS. Supplement (SM 3).

In Vitro Cytotoxicity Assays

The cytotoxicity of free PTX, blank liposomes, APNs, and L-APNs was assessed using the MTT assay. Cells were exposed to the formulations at varying concentrations, incubated for 24 and 48 h, treated with MTT solution, and absorbance was measured at 570 nm by using a microplate reader. Supplement (SM 4).

Cell Cycle Analysis

The DNA content of cells was measured using flow cytometry, and the percentage of cells resident in each cell cycle phase was evaluated using BD FACS Comp^{TM} software. Supplement (SM 5).

Pharmacokinetics, Biodistribution and Tumor Accumulation

To measure *in vivo* pharmacokinetic and tumor accumulation parameters, 4-week-old male BALB/c mice and tumor bearing C57BL6 mice, weighing 20–25 g were used respectively. For pharmacokinetic study, eighteen mice were divided into 3 groups with 6 mice in each group. For biodistribution study, twelve mice were separated into three experimental groups of 4 mice per group that received free PTX, APNs and L-APNs at a dose of 5 mg/kg (100 μL of a 1 mg/mL solution) *via* intravenous injection. The blood and organ samples were collected, processed, and analyzed *via* LC-MS/MS. The pharmacokinetic profiles for the free drug and for the formulations were fit to a non-compartmental model using WinNonLin software (v 2.0, Pharsight Software, Mountain View, CA). Supplement (SM 6).

Statistical Analyses

Data are expressed as the mean and standard error of four separate determinations. Analysis of variance (ANOVA) or a *t*-test was used to determine whether differences between test groups were statistically significant, with a '*p*' value less than 0.05 considered as a statistically significant difference.

RESULTS

Characterization of Liposome-Encapsulated Albumin-Paclitaxel Nanoparticles (L-APN)

The APN formulation was prepared by desolvation technique by maintaining 1% ethanol concentration. The average particle size of the resulting formulation was ~105 nm with a narrow size distribution. This is slightly smaller than Abraxane® nanoparticles (130 nm) and other nanomedicines, including Doxil® (150 nm) (25). Based on preliminary optimization, a fixed 3:150 M ratio of BSA to PTX (200:130 μg/mL concentration) gave the smallest particle size. At this ratio, roughly 6 molecules of PTX were observed to be bound at site 1 of BSA subdomains IIA and IIIA, resulting a ~10-fold increase in the particle size compared to blank BSA NPs (~10 nm) (26,27).

The L-APN formulation was prepared by a thin film hydration-extrusion technique. Specifically, a thin lipid film was hydrated with an aqueous solution that contained the preformed APNs, and the mixture was extruded through 200 nm porous membrane (Table I). The average particle size of L-APNs was ~210 nm with a uniform size distribution (PDI, ~0.090). These were larger than that of blank liposomes, suggesting that the APNs was loaded within the vesicular structure (Fig. 2). The blank liposomes showed a strong positive charge around 24 mV, with L-APNs having a considerably smaller charge of ~4 mV. This difference may reflect the partial compensation of the positive charge of the blank liposomes by the negative charge of APNs, which is attributed to pH higher than the isoelectric point of BSA and as well as to PTX binding. Consequently, the encapsulation efficiency (EE) and loading capacity were found to be ~99% and ~6.5%, respectively, for the L-APN formulation.

Morphology Analysis

TEM imaging further confirmed the size of the L-APNs in the dried state, as well as their structural morphology in all three special spatial dimensions after staining (Fig. 2). Specifically, the particles were characterized as distinct, discreet, and monodispersed spherical shapes for all the L-APNs examined; these findings were consistent with DLS observations. Notably, L-APNs exhibited a well-defined spherical morphology, whereas APNs were clearly spotted. In some cases, larger particles were observed, which probably represent either particle clusters or conglomerates formed after the evaporation of solvent. Although the shape observed with TEM was consistent with DLS evaluations, the size by TEM was smaller than that by DLS. This discrepancy is likely due to the fact that DLS measurement reflects the hydrodynamic particle size in its swollen state whereas TEM measures the diameter in the dried state.

Solid-State Characterizations

FT-IR spectroscopy was used to evaluate the chemical interactions among drug and protein/liposome functional groups. The spectra of free PTX, APNs and L-APNs are shown in (Fig. 3a). The PTX particles exhibited characteristics peaks at 2,965 cm^{-1} (=C–H), 1,707 cm^{-1} (C=O group), 1,641 cm^{-1} (C–C stretch), 1,370 cm^{-1} (CH_3 bending), 1,248 cm^{-1} (C–N

Table I Physicochemical Characteristics of APNs and L-APNs

	Particle size (nm)	PDI	ζ- Potential (mV)	Encapsulation efficiency (%)	Loading capacity (%)
APNs	106.2 ± 3.12	0.101 ± 0.02	−2.65 ± 0.986	–	–
Blank liposome	179.5 ± 2.13	0.086 ± 0.01	23.96 ± 0.381	–	–
L-APNs	209.7 ± 4.17	0.090 ± 0.03	3.69 ± 1.265	99.96 ± 0.01	6.5 ± 0.10

Data are expressed as mean ± SD ($n = 3$)

stretch), 1,072 cm^{-1} (C–O stretch), and 709 cm^{-1} (C–H off the plane) (28). Since these peaks were also present and largely unchanged in the spectra of the liposomal formulations, there were most likely no chemical interactions between PTX and the protein or liposome.

The DSC thermograms of free PTX, APNs, and L-APNs are presented in (Fig. 3b). Free PTX showed a sharp endothermic peak at 224°C, corresponding to its crystalline nature. The disappearance of this transition in both the APN and L-APN formulations implies that PTX is in a more amorphous molecular state. Most likely, hydrophobic interactions between PTX and BSA help to stabilize the amorphous form and encourage encapsulation in a vesicular structure, which is critical for achieving maximum entrapment efficiency. The XRD patterns of free PTX, APNs, and L-APNs are presented in (Fig. 3c). The XRD diffractogram of free PTX showed numerous sharp and intense peaks at scattering angles (2θ) of 10.81, 11.92, 12.90, 15.26, 16.81, 21.56, 25.089, 42.16°, implying a high level of crystallinity. In contrast, the diffraction patterns of APNs and L-APNs formulations did not exhibit these peaks, again indicating the presence of the drug in a largely amorphous form.

Liposomal Encapsulation of APNs by Size Exclusion Chromatography (SEC)

The SEC results confirmed that the APNs were incorporated inside the liposomes resulting in the L-APN formulation (Fig. 4). Specifically, free albumin eluted at a retention time of 4.417 min with an intensity of 500, and blank liposomes eluted at a retention time of 2.703 min with an intensity of 600. L-APNs eluted as two discrete peaks: one at a retention time of 2.703 min and an intensity of 1,200, and the second at a retention time of 4.417 min and an intensity of 150. This result strongly suggested that more than 90% of the APNs were incorporated inside the liposomes.

Colloidal Stability

Dilution-induced aggregation or dissociation was assessed by DLS and SEC. The particle size of the ANP formulation immediately began to increase upon dilution into water (Fig. 5a), by a factor of up to 20 at the highest dilution. In contrast, the particle size of the L-APN formulation remained constant upon dilution. Consistently, the intact L-APNs were readily detectable by SEC at the higher dilutions, while the intact ANPs was not detected at the corresponding dilutions (Fig. 5b). Upon long-term storage at 4 and 25°C, both APN and L-APN were very stable for 1 month in either PBS (phosphate buffer saline, 100 mM NaH_2PO_4, 150 mM NaCl, pH 7.4) or serum media (Fig. 5c).

In Vitro Release Kinetics

The *in vitro* release profiles of APNs and L-APNs are presented in (Fig. 6a and b). As expected, neither of the formulations showed an initial burst of drug release, indicating strong albumin-PTX interactions. APNs showed a biphasic release profile, with 20% of the total PTX released within the first 12 h, followed by a slow release of an additional 26% over the

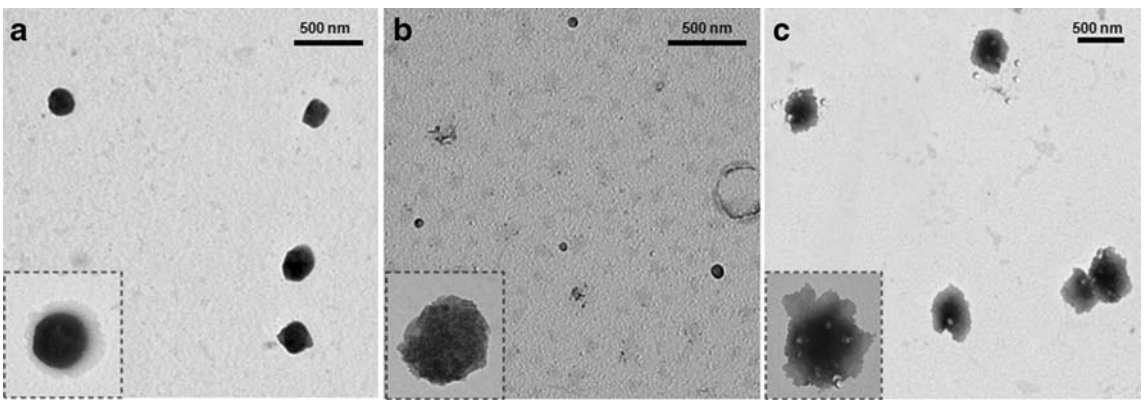

Fig. 2 TEM images of (**a**) blank liposomes, (**b**) APNs, and (**c**) L-APNs.

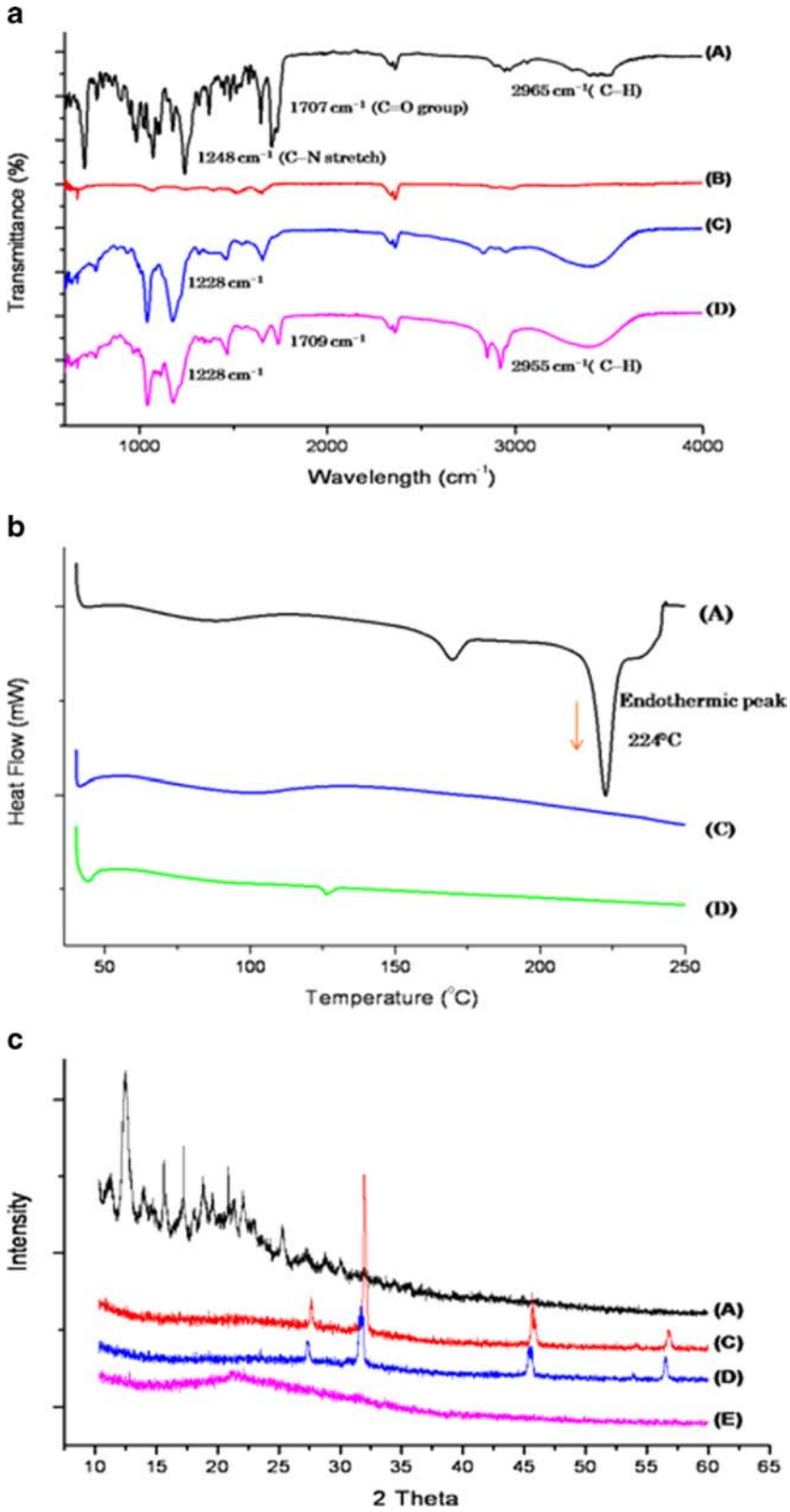

Fig 3 Solid state characterization of each formulation: (**a**) FT-IR (**b**) DSC thermograms (**c**) X-RD. Samples in each panel are (*A*) free PTX, (*B*) free albumin, (*C*) APNs, (*D*) L-APNs, and (*E*) blank liposomes.

next 72 h and up to 75% released after 7 days. This profile could be due to an initial release phase of the drug that was present on the surface of the nanoparticles (loose physical binding), with the drug within particles releasing more slowly. In contrast, L-APNs showed an apparently monophasic sustained release throughout the study period, with 6% of

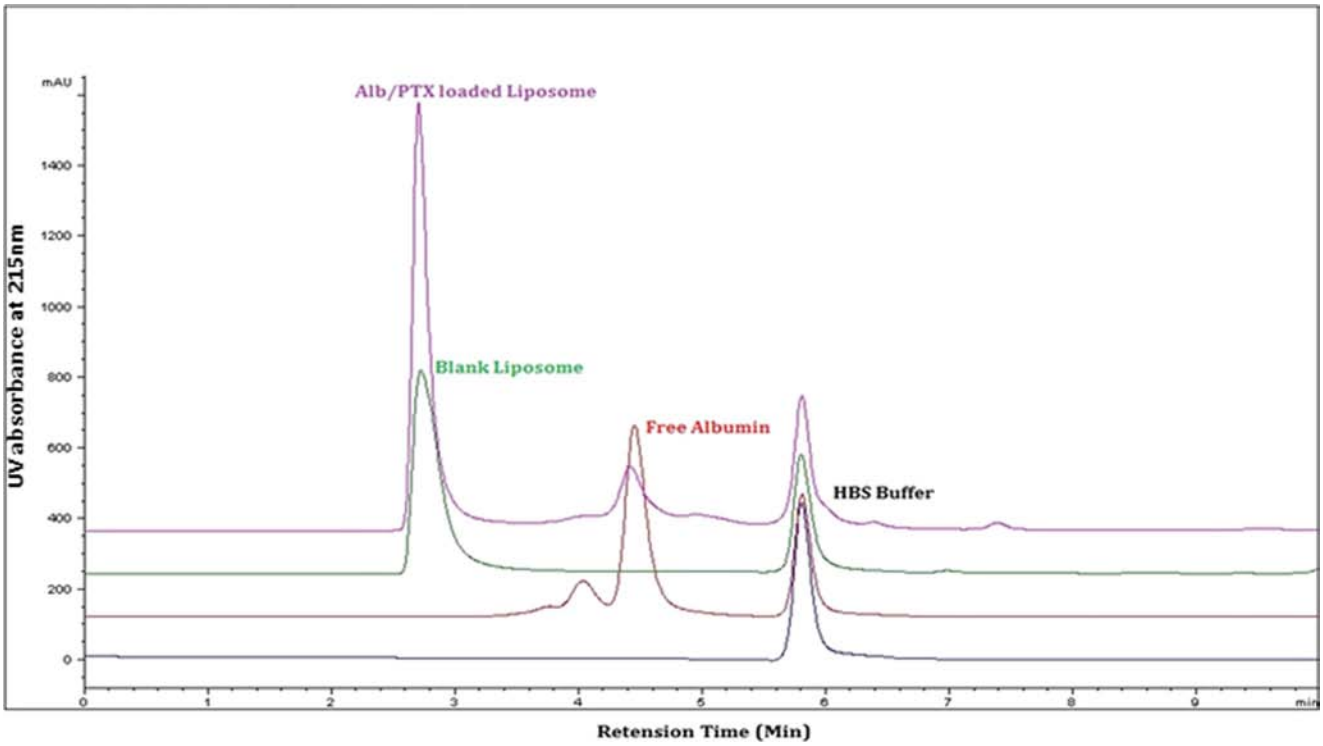

Fig 4 SEC of the different formulations. Blank HBS buffer (*blue*), free albumin (*red*), blank liposome (*green*), L-APN (*pink*).

PTX released in the first 12 h, 10% at the end of 24 h, and up to 30% released after 7 days. The slow release rate is likely due to the longer path length of PTX within the carrier. That is, PTX has to first detach from the hydrophobic core of albumin and then diffuse through the liposomal bilayer. This release profile could be advantageous in a patient, in that it effectively increases drug solubility, protects the drug, and has a significantly prolonged release profile at physiological pH values, thereby facilitating the occurrence of the EPR phenomenon (29,30). In addition, the prolonged serum half-life could increase the likelihood of perfusion into tumor interstitial tissue (31).

To analyze the profiles for the release kinetics, the data for both formulations was fit to Higuchi's model. The PTX release profiles plotted against the square root of time over the first 24 h resulted in more linear plot for L-APNs than that for APNs, indicating a controlled release phenomenon for the former. The data were also fit to the Korsmeyer-Peppas equation, wherein the exponent '*n*' is indicative of the release mechanism (32). Based on our data, the *n* value for L-APNs was 0.65 (Table S1), which corresponds to non-Fickian kinetics and likely indicates that more than one mechanism was involved in PTX release, probably diffusion and erosion.

Cytotoxicity Assay

The cytotoxicity of the blank nanoparticle towards B16F10 and MCF-7 cells was assessed by MTT assay after incubation for 24 or 48 h in the presence of the formulation at concentrations ranging from 0.001–10 μg/mL (Fig. 7a and b). No cytotoxicity was observed for blank nanocarriers with either cell line, even after 48 h incubation. This suggests that the carrier is completely biocompatible and suitable for further *in vivo* evaluation. In contrast, both APN and L-APNs showed measurable cytotoxicity that was dose and time-dependent. Both APNs and L-APNs were cytotoxic in a concentration range that corresponded to predicted plasma levels in humans (0.001–10 μg/mL) (33). Notably, APNs and L-APNs appeared to be slightly more cytotoxic than free PTX in both cell lines.

Cell Cycle Analysis

The cytotoxic effects of free PTX, APNs, and L-APNs were further investigated by cell cycle analysis in MCF 7 cells after incubation for 6 or 24 h at the concentration of 0.1 or 1 μg/ml PTX (Fig. 8). PTX binds to the α, β-tubulin dimer within the microtubules and thereby induces G_2/M arrest of rapidly dividing cells, and eventually apoptosis. In the present study, PTX did appear to have arrested cell growth at the G_2/M phase in a concentration- and time-dependent manner. The fraction of cells in the G_1 phase was considerably reduced with accumulation of G_2/M -phase cells at all time points evaluated. Interestingly, the percentage of cells in the G_2/M phase was also increased for the PTX nanoparticle formulations, which resulted in enhanced apoptosis. Interestingly, L-APNs induced a higher percentage of sub-G_1 cells than the other formulations: 12.29% after 6 h, compared to 3.27% and 2.18% for APN and free PTX, respectively. After 24 h

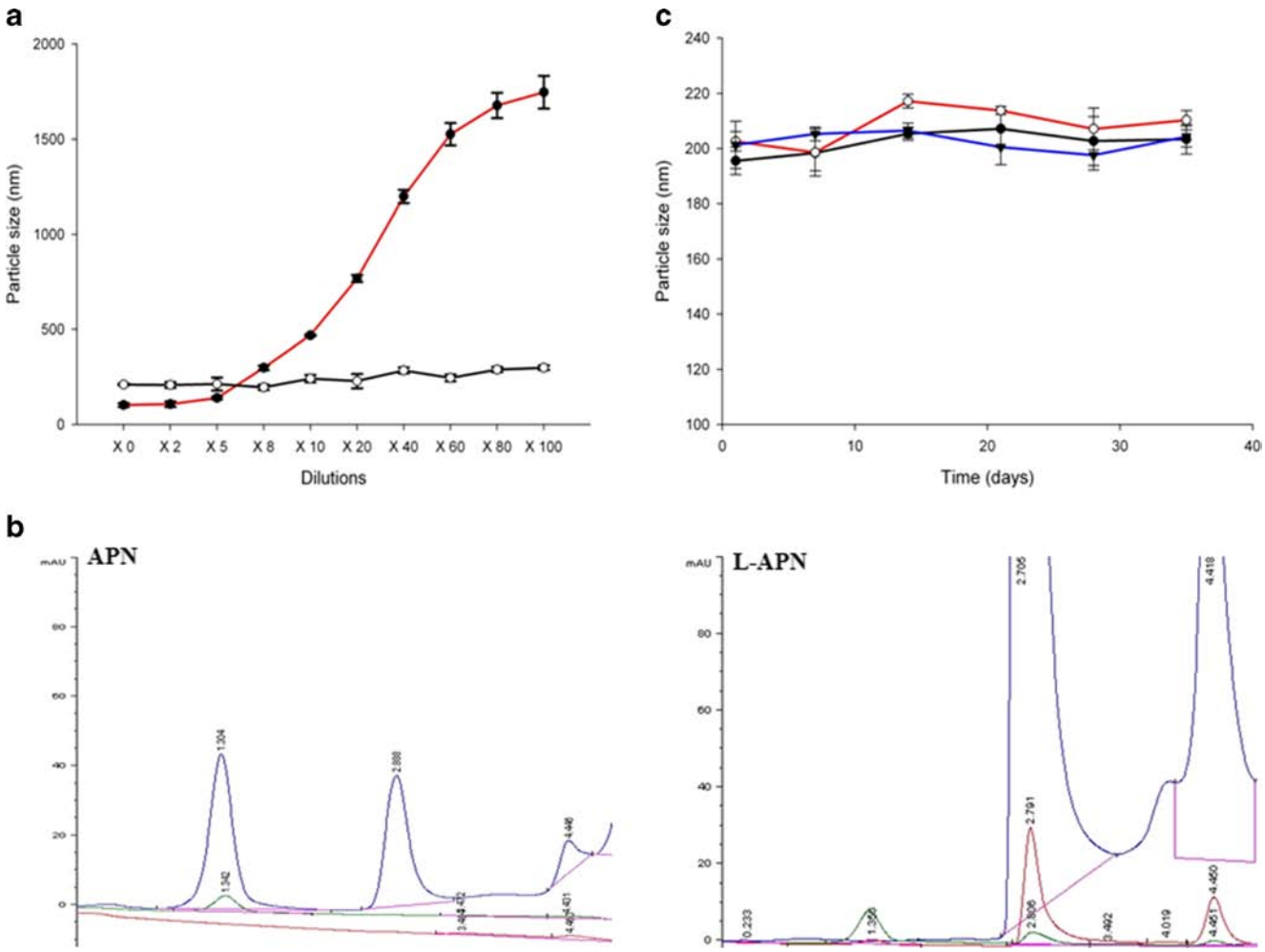

Fig 5 Colloidal stability after dilution of APNs (●) and L-APNs (○) determined by (**a**) DLS and **(b)** SEC (blue: non-diluted; red: 10-fold dilution; and green: 100-fold dilution). **(c)** Stability of L-APNs after storage at 25°C (○), 4°C (●), or serum (▼). Each value represents the mean ± SD ($n = 3$).

exposure to each formulation (1 μg/ml PTX), the proportion of apoptotic cells increased to 35%, 7.75%, and 6.78% for L-APN, APN, and PTX, respectively. The enhanced apoptosis observed for the L-ANP formulation may indicate that the liposomal components may influence PTX toxicity. At any rate, this enhancement of PTX activity could be a very promising improvement for treating clinical patients.

Cellular Uptake (CSLM, FACS & LC-MS/MS)

The cellular uptake of blank liposomes, APNs and L-APNs into B16F10 and MCF-7 cells was qualitatively assessed with flow cytometry (FACS) and confocal laser scanning microscopy (CLSM), using Alexa Fluor® 488-conjugated albumin and rhodamine-conjugated phospholipid (Rh-PE). As shown in (Fig. 9a), FACS analysis indicated that the fluorescence intensity of both cell types was increased after treatment with all formulations, indicating nanoparticle uptake. Notably, the uptake of L-APNs was significantly higher than both blank liposomes and APNs in both cell lines. The higher cellular uptake of L-APNs was also confirmed by CLSM. Initially, L-APNs appeared to accumulate in the cytoplasm, after which they distributed into the surrounding regions, including the nucleus. At equilibrium, the majority of green and red fluorescence was located in the cytoplasmic region (Fig. 9b). Based on these observations, it is likely that the nanoparticles are initially taken up *via* endocytosis into the late endosome region, followed by dissociation of the nanoparticles and diffusion through the cytoplasm, where the drug can presumably act on microtubules.

The cellular uptake of PTX into B16F10 and MCF-7 cells after treatments with the blank liposomes, APNs and L-APNs was quantitatively assessed with LC-MS/MS as a function of time. The cellular uptake of PTX increased in a time-dependent manner after treatment with APNs or L-APNs in both cell lines (Fig. 9c), with higher uptake observed into B16F10 cells. The maximum PTX concentration measured after L-APN treatment was 12.55 and 18.28 ng/mL for MCF-7 and B16F10 cells, respectively. Additionally, L-APNs showed

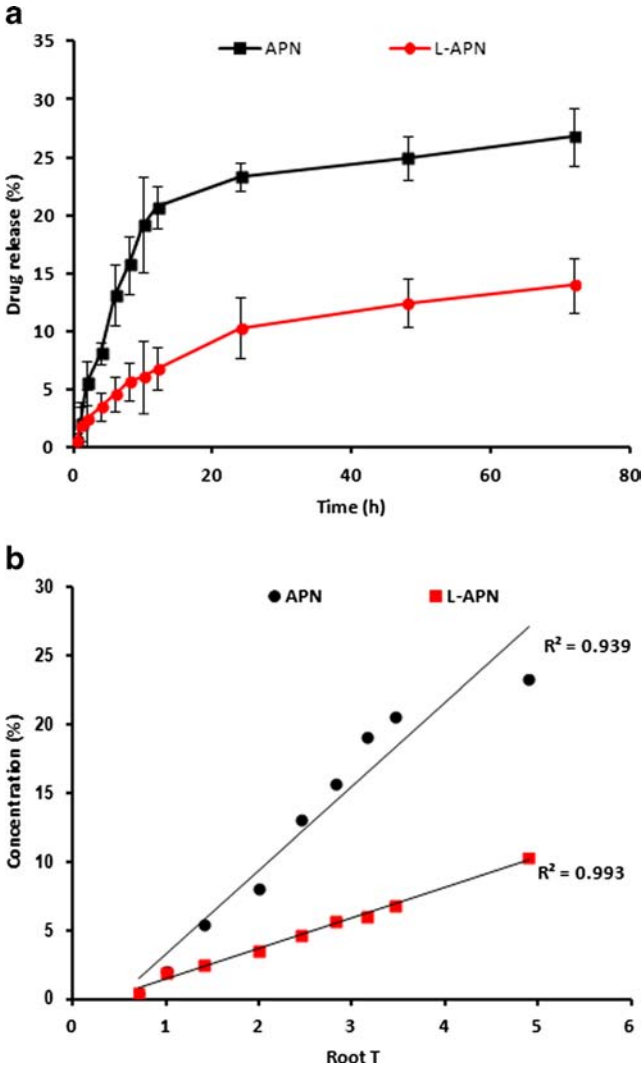

Fig 6 (**a**) *In vitro* release profiles of PTX from APNs and L-APNs in PBS buffer (pH 7.4, 0.14 M NaCl) at 37°C. (**b**) Higuchi plot of APNs and L-APNs. Data are expressed as mean ± SD ($n = 3$).

significantly higher uptake than that of APNs in both cell lines at all-time points measured. Consistent with the FACS analysis, LC-MS/MS analysis confirmed the time-dependence of the intracellular concentration of PTX after L-APN treatment. PTX concentration increased over the 2 h immediately after treatment but decreased thereafter. Specifically, in MCF-7 cells, the PTX concentration was 3-fold higher after 1 h than after 30 min, but remained relatively constant up to 2 h. This could be due to the initial flux internalization of the L-APNs into the cellular population, after which the apparent cellular uptake does not increase because most cells have already internalized the formulation. A similar trend was observed in B16F10 cells, with a 2-fold increase within 60 min followed by very little increase up to 120 min.

Pharmacokinetic Analysis, Biodistribution and Tumor Accumulation

The plasma concentration-time profiles of PTX were determined after a single intravenous dose of each formulation (5 mg/kg) in mice. After an initial burst, the plasma concentration of PTX was rapidly decreased with either free PTX or APNs, characterized by a biphasic initial distribution phase followed by a rapid elimination phase to less than 2 ng/mL within 8 h (Fig. 10a). The PTX clearance was similar for both free PTX and APNs. This result is consistent with our *in vitro* colloidal stability analysis in which APNs showed rapid dissociation in plasma. Importantly, after administration of a single L-APN dose, PTX remained in the bloodstream at concentrations higher than those of APNs throughout the time course. Pharmacokinetic parameters estimated by non-compartmental analysis are shown in Table II. The $AUC_{0-\infty}$ for L-APNs was 668.01 ng/L·h, which is 4-fold higher than that of either free PTX or APNs ($p < 0.0001$). L-APNs also had a 3- to 4-fold lower clearance, 1.5- to 2-fold greater mean retention time, longer plasma half-life, and lower elimination rate constant than either free PTX or APNs. The *in vivo* tissue distribution of PTX was also evaluated in B16F10 tumor-bearing mice after *i.v* injection of free PTX, APNs, and L-APNs (5 mg/kg PTX) (Fig. 10b). The PTX was rapidly distributed in all major organs following the i.v injection, with highest concentration of drug was observed in liver, followed by kidney and lungs. Notably, L-APN preferentially accumulated in the tumor by comparison to free PTX and APN.

DISCUS?SION

PTX is a microtubule inhibitor approved for the treatment of various cancer types, including breast, ovarian, non-small cell lung cancer, and head and neck carcinomas. To address the challenges of PTX solubility and vehicle toxicity, several nanoparticle-based formulations of PTX have been developed, including Taxol® and Abraxane®. Although both have been partially successful, neither addressed the pharmacokinetic challenges of PTX, most notably its rapid elimination from systemic circulation. The poor colloidal stability of the nanoparticulate formulations in blood circulation is attributed to their poor *in vivo* performance. To address these challenges, we have proposed the liposome-encapsulated albumin-PTX nanoparticles (L-APNs). In principle, this should provide *in vivo* colloidal stability to the otherwise unstable albumin-PTX nanoparticles in the bloodstream and should thereby prolong the plasma half-life (34).

In vitro analyses of L-APN confirmed that PTX was in an amorphous and molecularly dispersed state that should be readily released in target tissues after i.v. administration. In

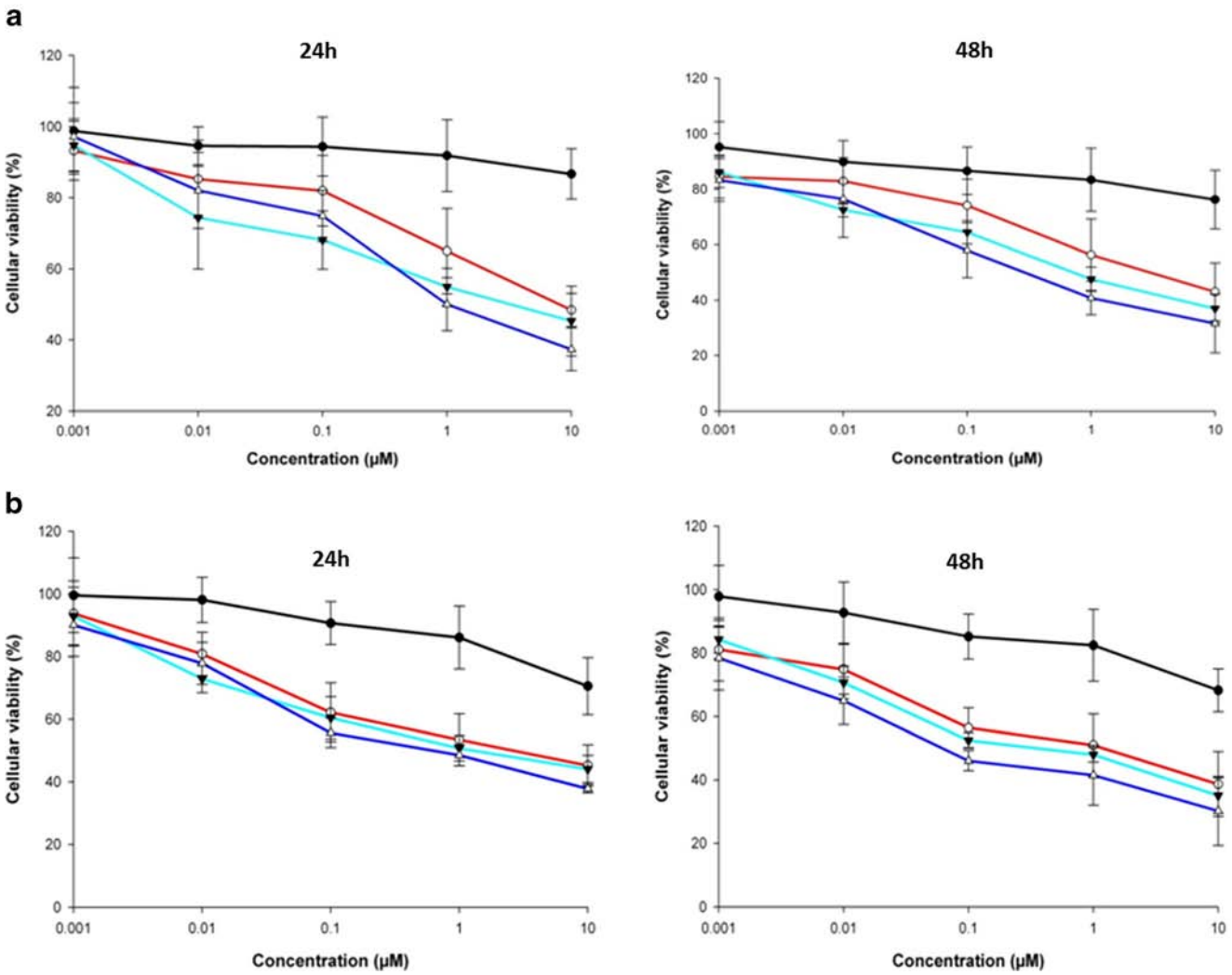

Fig 7 *In vitro* cytotoxicity of drug-free nanoparticles (● *black*), free PTX (○red), APNs (▼ *light blue*), and L-APNs (Δ *dark blue*) in (**a**) B16F10 and (**b**) MCF-7 cells after 24 and 48 h incubation. Each value represents the mean ± SE ($n = 8$).

addition, L-APNs showed better colloidal stability by comparison to APNs. The poor colloidal stability of APNs reflects the dissociation of PTX and albumin due to the lack of any protective entangling interactions, whereas the exceptional stability of L-APN reflects the stabilizing effect by the liposomal coating and the hydrophilic PEG tails (scheme S1). This high stability is predictive of a long serum half-life *in vivo*, increased accumulation in tumor tissues, and better control of drug release.

A PTX-loaded nanocarrier capable of protecting the drug from rapid elimination while maintaining the cytotoxic activity would be of particularly high therapeutic interest (31). Although PTX is hydrophobic overall, it does have significantly hydrophilic regions consisting of multiple hydroxyls and secondary amines. Because of this, it is likely that PTX bound to a polymer *via* functional group interactions could release rapidly in a physiological environment, with an associated burst of cytotoxic activity (35). Following this initial burst, the drug should be released from the core structure over an extended time period, with associated prolonged cytotoxic activity. It has been reported that at longer incubation periods, a larger number of cells enter the G_2/M cell cycle phases after treatment with active PTX (36). In general, free PTX can diffuse directly into cell nuclei, whereas a drug-carrier complex would be retained in the late endosomal structure or cytosol for an extended time prior to drug release and diffusion to the nucleus (37). Since the site of action for PTX is in the cytosol, the higher cytosolic residency time of the nanoparticles formulations could result in higher cytotoxic activity. Our CLSM and cytotoxicity analyses confirmed this behavior for the L-APN formulation. It should be noted that the higher toxicity could also be due to some cytotoxicity associated with the carrier nanoparticles (15–20% cytotoxicity) (38).

Cell-mediated endocytosis seems to be the principle basis for the high cellular uptake and enhanced cytotoxic action of

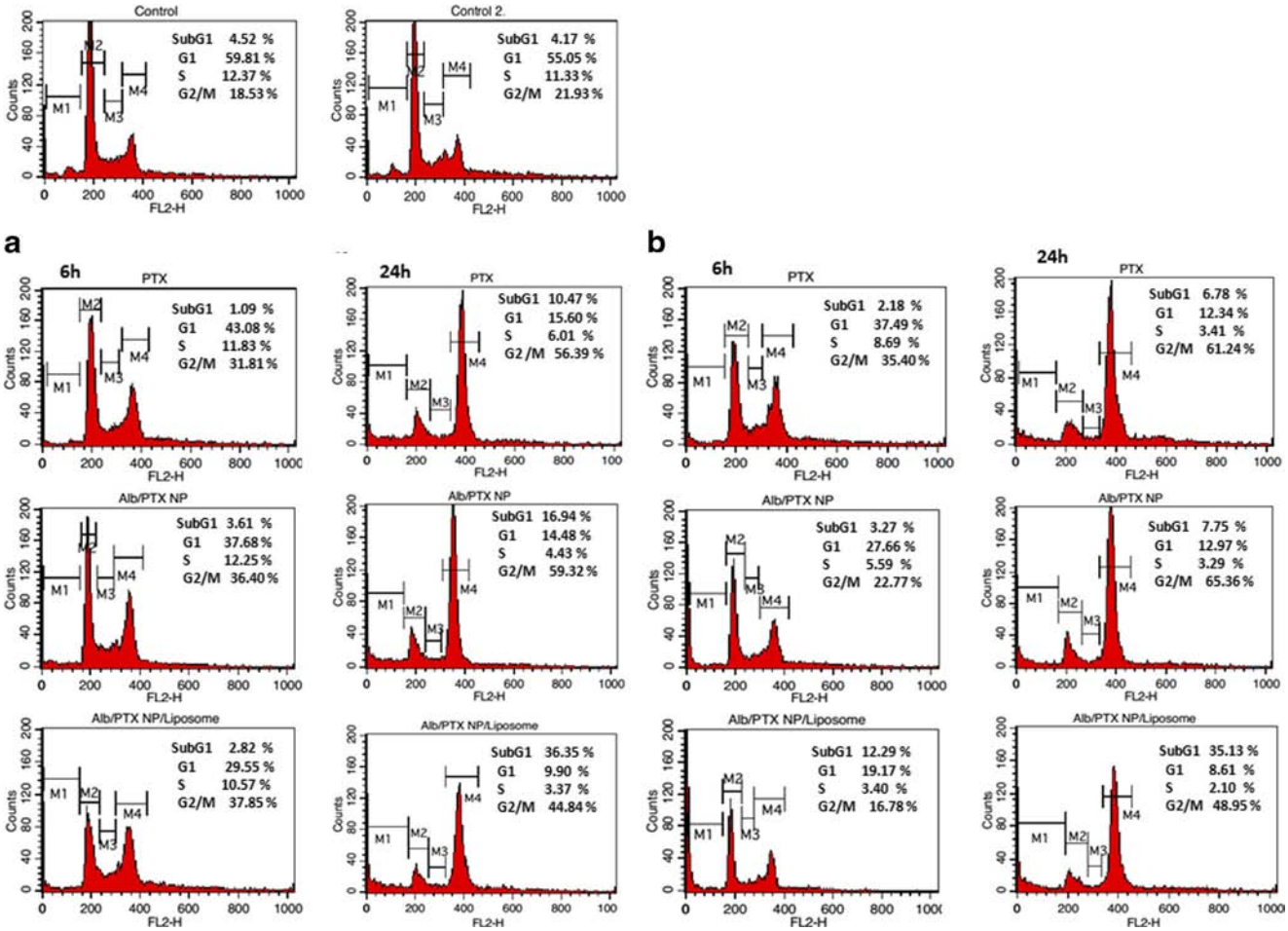

Fig 8 Cell cycle analysis after treatment with free PTX, APNs, or L-APNs in MCF 7 cells at (**a**) 0.1 μg/mL or (**b**) 1.0 μg/mL after 6 and 24 h incubation, respectively. A representative set of data from three independent experiments is shown. Cells were harvested and cell cycle phases were analyzed using flow cytometer. G_0/G_1, G_2/M, and S indicate the cell phase, and sub-G_0/G_1 refers to the proportion of apoptotic cells.

L-APNs (39). The higher cellular uptake of L-APNs can be partially explained by the interaction of the positively charged DOTAP liposomes with the negatively charged cell membrane, resulting in immediate endocytosis of the nanoparticles. Furthermore, the hydrophobic nature of the nanoparticle complex could facilitate its internalization into the cell membrane (40). It should be noted that cellular uptake was not affected by the presence of brush-like PEG tail around the nanoparticles. Additionally, our observation that fluorescent probes associated with both the albumin protein and the liposomal lipids were localized to the cytoplasm implies that the L-APN assembly remained intact in the media and through the endocytotic process. Finally, our LC-MS/MS analysis indicated a higher net cellular uptake of PTX from L-APNs than APNs. This phenomenon could mainly be attributed to the difference in surface charge between the formulations. That is, the positively charged L-APNs were readily internalized by the negatively charged cancer cell membrane owing to charge-based affinity (29).

The L-APNs also had a significantly improved *in vivo* behavior, most notably a longer plasma half-life. This highlights the important benefits of entrapping the APNs into the PEGylated liposomal carrier. Most likely, the PEG moiety on the liposomal surface increases steric repulsion and shielding efficiency, by forming a hydrating layer that covers the particles, thereby inhibiting plasma protein binding to minimize the opsonization and subsequent macrophage uptake (29,41). Additional contributing factors to the prolonged half-life may include the small particle size (~200 nm), uniform size distribution (~0.2 PDI), high physical/colloidal stability in plasma, tunable/controlled release of drugs, and protection of albumin-PTX within the stable liposomal carrier (36,42,43). In principle, the improved pharmacokinetic properties of L-APNs should translate to improved anti-tumor efficacy, particularly given the likelihood of an enhanced EPR effect (44), which was confirmed by preferential accumulation of PTX by L-APNs. The tumor accumulation studies depicted a prolonged blood circulation, reduced RES

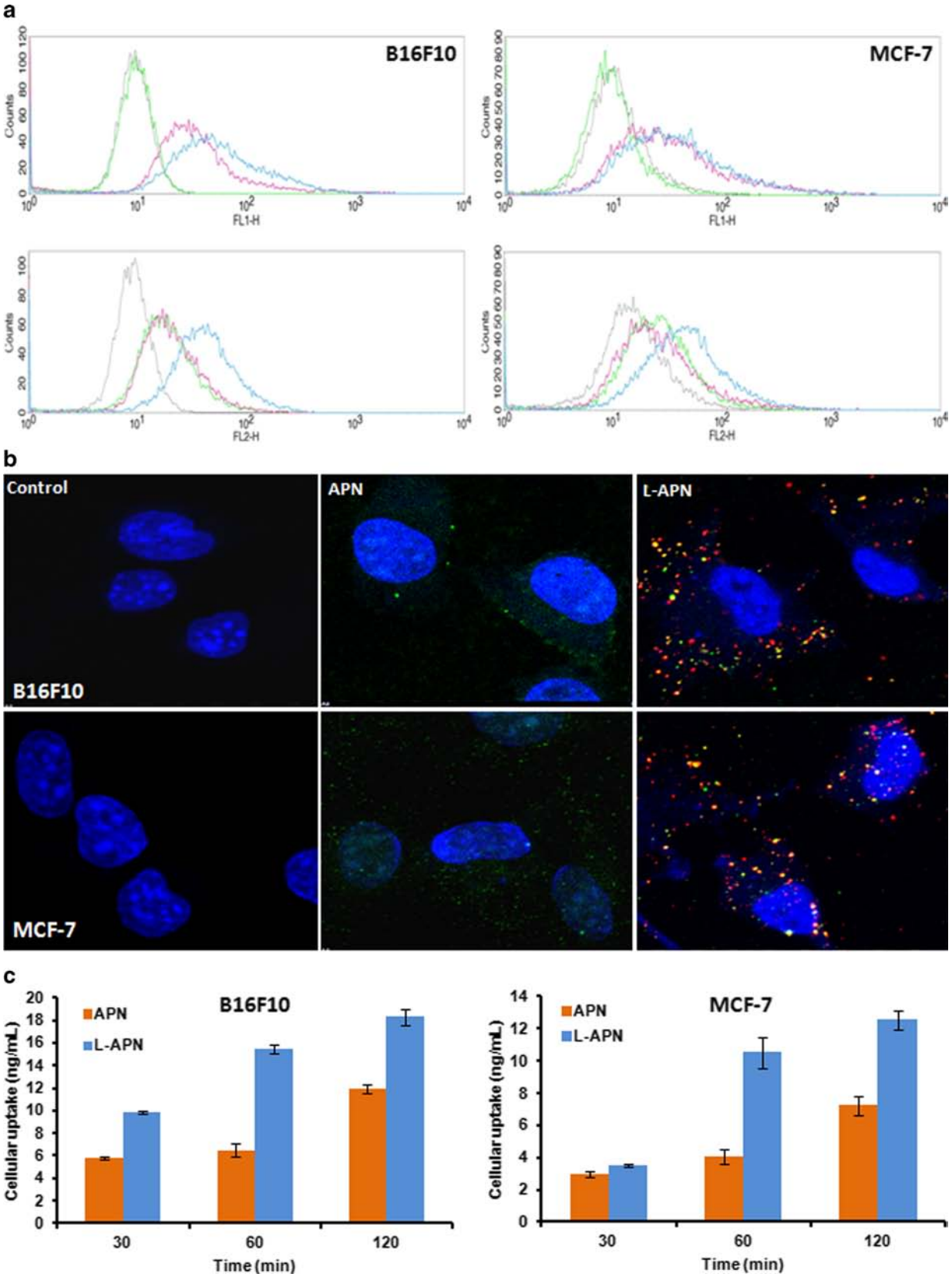

Fig 9 *In vitro* cellular uptake of various formulations into B16F10 and MCF7 cells. (**a**) FACS analysis of fluorescently labeled drug-free nanoparticles (*green*), APNs (*pink*), and L-APNs (*blue*) *via* FL1 and FL2 channels. (**b**) CLSM analysis of cells after treatment with drug-free nanoparticles, APNs and L-APNs (Hoechst dye: *blue*, AlexaFluor® 488-albumin: *green*, and rhodamine-phospholipid: *red*). (**c**) Quantitative cellular uptake measured by LC-MS/MS.

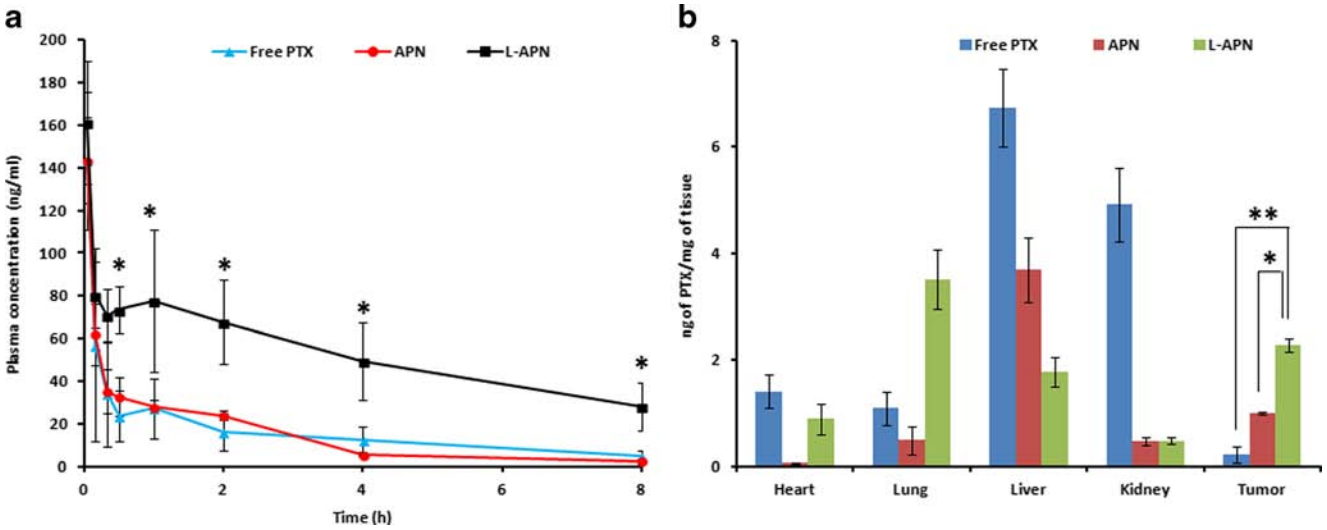

Fig. 10 (**a**) Plasma concentration–time profiles after administration of a single intravenous 5 mg/kg dose of free PTX, ANPs and L-ANPs in mice. (**b**) Biodistribution and Tumor accumulation profile of free PTX, ANPs and L-ANPs in tumor mice after 2 h of intravenous administration. Values reported are the mean ± SE ($n = 4$). *$P < 0.0001$, compared to that of APN **$P < 0.0001$, compared to that of PTX.

uptake, and relatively higher tumor accumulation for L-APN after i.v. administration of formulations. Preferential accumulation of PEGylated liposome in tumor was attributed to the EPR effect, depot effect (sustained release) and low systemic clearance. In addition, low presence of L-APN in liver was suggestive of reduced RES uptake while higher accumulation in lungs due to its bigger particle size. The higher localization of free PTX and APN in liver and kidney was consistent with the RES uptake as reported by Rowinsky and Donehower (45). Interestingly, low tumor accumulation of free PTX was attributed to the rapid metabolization of active compound and elimination *via* kidney resulting to poor localization in tumor region (consistent with the PK analysis) (46). The APN was also expected to meet the same fate due to its poor *in vivo* colloidal stability leading to disassembly of PTX and albumin in blood circulation.

Table II Pharmacokinetic Parameters of PTX After Intravenous Administration of free PTX, APNs, and L-APNs to Mice (5 mg/kg). Data are Expressed as Mean ± SE ($n = 4$ per Treatment)

Parameters	Free PTX	APN	L-APN
AUC_{0-8h} (h·μg /ml)	0.14 ± 0.12	0.19 ± 0.18	0.43 ± 0.27*
$AUC_{0-\infty}$ (h·μg /ml)	0.17 ± 0.14	0.12 ± 0.16	0.67 ± 0.53*
Cl ((mg/kg)/(μg/mL)/h)	0.73 ± 0.31	0.84 ± 0.12	0.21 ± 0.11*
C_{max} (μg/ml)	0.15 ± 0.04	0.14 ± 0.06	0.16 ± 0.05*
MRT (h)	1.77 ± 0.48	1.47 ± 0.43	3.05 ± 0.22*

C_{max} Maximum concentration, $AUC_{(0-8h)}$ Area under the curve up to the 8 h, $AUC_{(0-\infty)}$ AUC up to infinite time, *MRT* Mean residence time, *Cl* Clearance

*$P < 0.0001$, significant difference between L-APNs and APNs or free PTX

CONCLUSION

In summary, albumin-paclitaxel nanoparticles (APNs) were successfully incorporated into a liposomal bilayer, resulting in liposome-encapsulated APNs (L-APNs). The L-APNs showed sustained drug release and excellent colloidal stability in a physiological medium, even when significantly diluted. L-APNs also showed pronounced cytotoxic activity toward B16F10 and MCF-7 cells mediated by pronounced arrest at the G_2/M phase and an increased prevalence of sub-G_1 apoptotic cells. Finally, L-APNs showed remarkably enhanced blood circulation and tumor accumulation. Taken together, our results highlight L-APN as a promising carrier system of paclitaxel for further optimization and development towards the clinical applications.

ACKNOWLEDGMENTS AND DISCLOSURES

This research was supported by the Basic Science Research Program of Korean National Research Foundation (NRF-20110007794).

REFERENCES

1. Rowinsky EK, Cazenave LA, Donehower RC. Taxol: a novel investigational antimicrotubule agent. J Natl Cancer Inst. 1990;82(15):1247–59.
2. Singla AK, Garg A, Aggarwal D. Paclitaxel and its formulations. Int J Pharm. 2002;235(1):179–92.
3. Weiss RB, Donehower R, Wiernik P, Ohnuma T, Gralla R, Trump D, *et al.* Hypersensitivity reactions from taxol. J Clin Oncol. 1990;8(7):1263–8.
4. Akhlaghi SP, Saremi S, Ostad SN, Dinarvand R, Atyabi F. Discriminated effects of thiolated chitosan-coated pMMA

paclitaxel-loaded nanoparticles on different normal and cancer cell lines. Nanomedicine. 2010;6(5):689–97.
5. Bernabeu E, Helguera G, Legaspi MJ, Gonzalez L, Hocht C, Taira C, *et al.* Paclitaxel-loaded PCL–TPGS nanoparticles: In vitro and in vivo performance compared with Abraxane®. Colloids Surf B: Biointerfaces. 2014;113:43–50.
6. Gelderblom H, Verweij J, Nooter K, Sparreboom A. Cremophor EL: the drawbacks and advantages of vehicle selection for drug formulation. Eur J Cancer. 2001;37(13):1590–8.
7. Fan T, Takayama K, Hattori Y, Maitani Y. Formulation optimization of paclitaxel carried by PEGylated emulsions based on artificial neural network. Pharm Res. 2004;21(9):1692–7.
8. Huh KM, Min HS, Lee SC, Lee HJ, Kim S, Park K. A new hydrotropic block copolymer micelle system for aqueous solubilization of paclitaxel. J Control Release. 2008;126(2):122–9.
9. Chen DB, Yang TZ, Lu WL, Zhang Q. In vitro and in vivo study of two types of long-circulating solid lipid nanoparticles containing paclitaxel. Chem Pharm Bull. 2001;49(11):1444–7.
10. Wang X, Zhou J, Wang Y, Zhu Z, Lu Y, Wei Y, *et al.* A phase I clinical and pharmacokinetic study of paclitaxel liposome infused in non-small cell lung cancer patients with malignant pleural effusions. Eur J Cancer. 2010;46(8):1474–80.
11. Xiao K, Luo J, Fowler WL, Li Y, Lee JS, Xing L, *et al.* A self-assembling nanoparticle for paclitaxel delivery in ovarian cancer. Biomaterials. 2009;30(30):6006–16.
12. Xie Z, Guan H, Chen X, Lu C, Chen L, Hu X, *et al.* A novel polymer–paclitaxel conjugate based on amphiphilic triblock copolymer. J Control Release. 2007;117(2):210–6.
13. Gradishar WJ. Albumin-bound paclitaxel: a next-generation taxane. Expert Opin Pharmacother. 2006;7(8):1041–53.
14. Sparreboom A, Scripture CD, Trieu V, Williams PJ, De T, Yang A, *et al.* Comparative preclinical and clinical pharmacokinetics of a cremophor-free, nanoparticle albumin-bound paclitaxel (ABI-007) and paclitaxel formulated in Cremophor (Taxol). Clin Cancer Res. 2005;11(11):4136–43.
15. Devalapally H, Duan Z, Seiden MV, Amiji MM. Modulation of drug resistance in ovarian adenocarcinoma by enhancing intracellular ceramide using tamoxifen-loaded biodegradable polymeric nanoparticles. Clin Cancer Res. 2008;14(10):3193–203.
16. Koudelka S, Turanek J. Liposomal paclitaxel formulations. J Control Release. 2012;163(3):322–34.
17. Hyodo K, Yamamoto E, Suzuki T, Kikuchi H, Asano M, Ishihara H. Development of liposomal anticancer drugs. Biol Pharm Bull. 2013;36(5):703–7.
18. Ko YT, Falcao C, Torchilin VP. Cationic liposomes loaded with proapoptotic peptide D-(KLAKLAK) 2 and Bcl-2 antisense oligodeoxynucleotide G3139 for enhanced anticancer therapy. Mol Pharm. 2009;6(3):971–7.
19. Ewe A, Schaper A, Barnert S, Schubert R, Temme A, Bakowsky U, *et al.* Storage stability of optimal liposome–polyethylenimine complexes (lipopolyplexes) for DNA or siRNA delivery. Acta Biomater. 2014;10(6):2663–73.
20. Liu M, Gan L, Chen L, Xu Z, Zhu D, Hao Z, *et al.* Supramolecular core–shell nanosilica@ liposome nanocapsules for drug delivery. Langmuir. 2012;28(29):10725–32.
21. Ko YT, Kale A, Hartner WC, Papahadjopoulos-Sternberg B, Torchilin VP. Self-assembling micelle-like nanoparticles based on phospholipid–polyethyleneimine conjugates for systemic gene delivery. J Control Release. 2009;133(2):132–8.
22. Miyata K, Christie RJ, Kataoka K. Polymeric micelles for nano-scale drug delivery. React Funct Polym. 2011;71(3):227–34.
23. Bansal A, Kapoor D, Kapil R, Chhabra N, Dhawan S. Design and development of paclitaxel-loaded bovine serum albumin nanoparticles for brain targeting. Acta Pharma. 2011;61(2):141–56.
24. Paal K, Muller J, Hegedus L. High affinity binding of paclitaxel to human serum albumin. Eur J Biochem. 2001;268(7):2187–91.
25. Dreher MR, Liu W, Michelich CR, Dewhirst MW, Yuan F, Chilkoti A. Tumor vascular permeability, accumulation, and penetration of macromolecular drug carriers. J Natl Cancer Inst. 2006;98(5):335–44.
26. Trynda-Lemiesz L. Paclitaxel–HSA interaction. Binding sites on HSA molecule. Bioorg Med Chem. 2004;12(12):3269–75.
27. Trynda-Lemiesz L, Luczkowski M. Human serum albumin: spectroscopic studies of the paclitaxel binding and proximity relationships with cisplatin and adriamycin. J Inorg Biochem. 2004;98(11):1851–6.
28. Hiremath JG, Khamar NS, Palavalli SG, Rudani CG, Aitha R, Mura P. Paclitaxel loaded carrier based biodegradable polymeric implants: preparation and in vitro characterization. Saudi Pharm J. 2013;21(1):85–91.
29. Parveen S, Sahoo SK. Long circulating chitosan/PEG blended PLGA nanoparticle for tumor drug delivery. Eur J Pharmacol. 2011;670(2):372–83.
30. Ernsting MJ, Murakami M, Undzys E, Aman A, Press B, Li SD. A docetaxel-carboxymethylcellulose nanoparticle outperforms the approved taxane nanoformulation, Abraxane, in mouse tumor models with significant control of metastases. J Control Release. 2012;162(3):575–81.
31. Araki T, Kono Y, Ogawara KI, Watanabe T, Ono T, Kimura T, *et al.* Formulation and evaluation of paclitaxel-loaded polymeric nanoparticles composed of polyethylene glycol and polylactic acid block copolymer. Biol Pharm Bull. 2012;35(8):1306–13.
32. Ramasamy T, Tran TH, Cho HJ, Kim JH, Kim YI, Jeon JY, *et al.* Chitosan-based polyelectrolyte complexes as potential nanoparticulate carriers: physicochemical and biological characterization. Pharm Res. 2014;31(5):1302–14.
33. Raymond E, Hanauske A, Faivre S, Izbicka E, Clark G, Rowinsky EK, *et al.* Effects of prolonged versus short-term exposure paclitaxel (Taxol (R)) on human tumor colonyforming units. Anti Cancer Drugs. 1997;8(4):379–85.
34. Jiang L, Xu Y, Liu Q, Tang Y, Ge L, Zheng C, *et al.* A nontoxic disulfide bond reducing method for lipophilic drug-loaded albumin nanoparticle preparation: formation dynamics, influencing factors and formation mechanisms investigation. Int J Pharm. 2013;443(1):80–6.
35. Lee IH, Park YT, Roh K, Chung H, Kwon IC, Jeong SY. Stable paclitaxel formulations in oily contrast medium. J Control Release. 2005;102(2):415–25.
36. Zhang L, He Y, Ma G, Song C, Sun H. Paclitaxel-loaded polymeric micelles based on poly (ε-caprolactone)-poly (ethylene glycol)-poly (γ-caprolactone) triblock copolymers: in vitro and in vivo evaluation. Nanomedicine. 2012;8(6):925–34.
37. Ramasamy T, Kim J, Choi HG, Yong CS, Kim JO. Novel dual drug-loaded block ionomer complex micelles for enhancing the efficacy of chemotherapy treatments. J Biomed Nanotechnol. 2014;10(7):1304–12.
38. Zhu Z, Li Y, Li X, Li R, Jia Z, Liu B, *et al.* Paclitaxel-loaded poly (N-vinylpyrrolidone)- b-poly (ε-caprolactone) nanoparticles: preparation and antitumor activity in vivo. J Control Release. 2010;142(3):438–46.
39. Cho HJ, Yoon IS, Yoon HY, Koo H, Jin YJ, Ko SH, *et al.* Polyethylene glycol-conjugated hyaluronic acid-ceramide self-assembled nanoparticles for targeted delivery of doxorubicin. Biomaterials. 2012;33(4):1190–200.
40. Termsarasab U, Cho HJ, Kim DH, Chong S, Chung SJ, Shim CK, *et al.* Chitosan oligosaccharide–arachidic acid-based nanoparticles for anti-cancer drug delivery. Int J Pharm. 2013;441(1):373–80.
41. Yang T, Cui FD, Choi MK, Cho JW, Chung SJ, Shim CK, *et al.* Enhanced solubility and stability of PEGylated liposomal paclitaxel: In vitro and in vivo evaluation. Int J Pharm. 2007;338(1):317–26.
42. Zhang W, Shi Y, Chen Y, Yu S, Hao J, Luo J, *et al.* Enhanced antitumor efficacy by paclitaxel-loaded pluronic P123/F127 mixed micelles against non-small cell lung cancer based on passive tumor targeting and modulation of drug resistance. Eur J Pharm Biopharm. 2010;75(3):341–53.

43. Ramasamy T, Kim JH, Choi JY, Tran TH, Choi HG, Yong CS, *et al.* pH sensitive polyelectrolyte complex micelles for highly effective combination chemotherapy. J Mater Chem B. 2014;2(37):6324–33.
44. Ko YT, Bhattacharya R, Bickel U. Liposome encapsulated polyethylenimine/ODN polyplexes for brain targeting. J Control Release. 2009;133(3):230–7.
45. Rowinsky E, Donehower R, editors. The clinical pharmacology of paclitaxel (Taxol). Semin Oncol. 1993;20(4–3):16-25.
46. Zhang C, Qu G, Sun Y, Wu X, Yao Z, Guo Q, *et al.* Pharmacokinetics, biodistribution, efficacy and safety of N-octyl-O-sulfate chitosan micelles loaded with paclitaxel. Biomaterials. 2008;29(9):1233–41.